JOURNAL OF SOLID STATE CHEMISTRY 89, 315–327 (1990)

Properties of the Transition Metal Dichalcogenides: The Case of IrS_2 and $IrSe_2$

S. JOBIC, P. DENIARD, R. BREC, AND J. ROUXEL

Institut de Physique et Chimie des Matériaux, Laboratoire de Chimie des Solides, 2 rue de la Houssinière, 44072 Nantes Cédex 03 France

M. G. B. DREW

Department of Chemistry, The University, Whiteknights, Reading RG6 2AD, U.K.

AND W. I. F. DAVID

Rutherford Appleton Laboratory, Chilton, Didcot, OX11 OQX, U.K.

Received March 30, 1990

The syntheses and structure determination of $IrSe_2$ and IrS_2 were undertaken. Pure phases were obtained and powder data were measured on an X-ray diffractometer. Rietveld refinement was successfully carried out for both structures [$IrSe_2$, 269 observations R (weighted profile) 0.062; IrS_2, 205 observations R (weighted profile) 0.074]. The *Pnam* space group (No. 62) was found to yield the best results, eliminating $Pna2_1$ as the other possible space group considered in a previous study of $IrSe_2$. Chalcogen pairs are found in both structures and these may correspond, in a first approach, to the charge balance $Ir^{3+}X^{2-}(X_2)^{2-}_{1/2}$. However, long bond lengths were found in the chalcogen pairs [S–S 2.299(11) Å, Se–Se 2.555(4) Å] along with an unexpectedly small effective cationic radius of 0.50 Å for Ir^{3+}. These features of IrS_2 and $IrSe_2$ are discussed.

Introduction

Most of the transition elements give dichalcogenides (*1, 2*), with good stoichiometry. In some cases, some nonstoichiometry can be found on the cationic sites [e.g., TiS_2 with an excess of titanium (3)] or on the anionic ones [e.g., $ZrSe_2$ with selenium vacancies (4)]. If one considers all the MX_2 binary phases (see Table I), via the position of the corresponding transition elements of the Periodic Table, it is possible to separate them in two main groups. The first group, situated on the left of the chart, contains the IVd, Vd and VId elements (with the exception of manganese), which form two-dimensional structures (2D) in their dichalcogenide compounds [see for instance (*2*) for all the phase polytypes]. The second group on the right of the table forms mostly tridimensional arrangements (3D) of the pyrite or marcasite type. This is in agreement with a destabilization of high oxidation states when going from the left to the right and from the bottom to the top of the table.

0022-4596/90 $3.00

TABLE I

CLASSIFICATION OF THE TRANSITION METAL DICHALCOGENIDES MX_2 SHOWING THE SEPARATION (THICK VERTICAL LINE) BETWEEN TWO-DIMENSIONAL PHASES (2D STRUCTURES ON LEFT) AND THE MOSTLY THREE-DIMENSIONAL PHASES (3D STRUCTURES ON RIGHT)

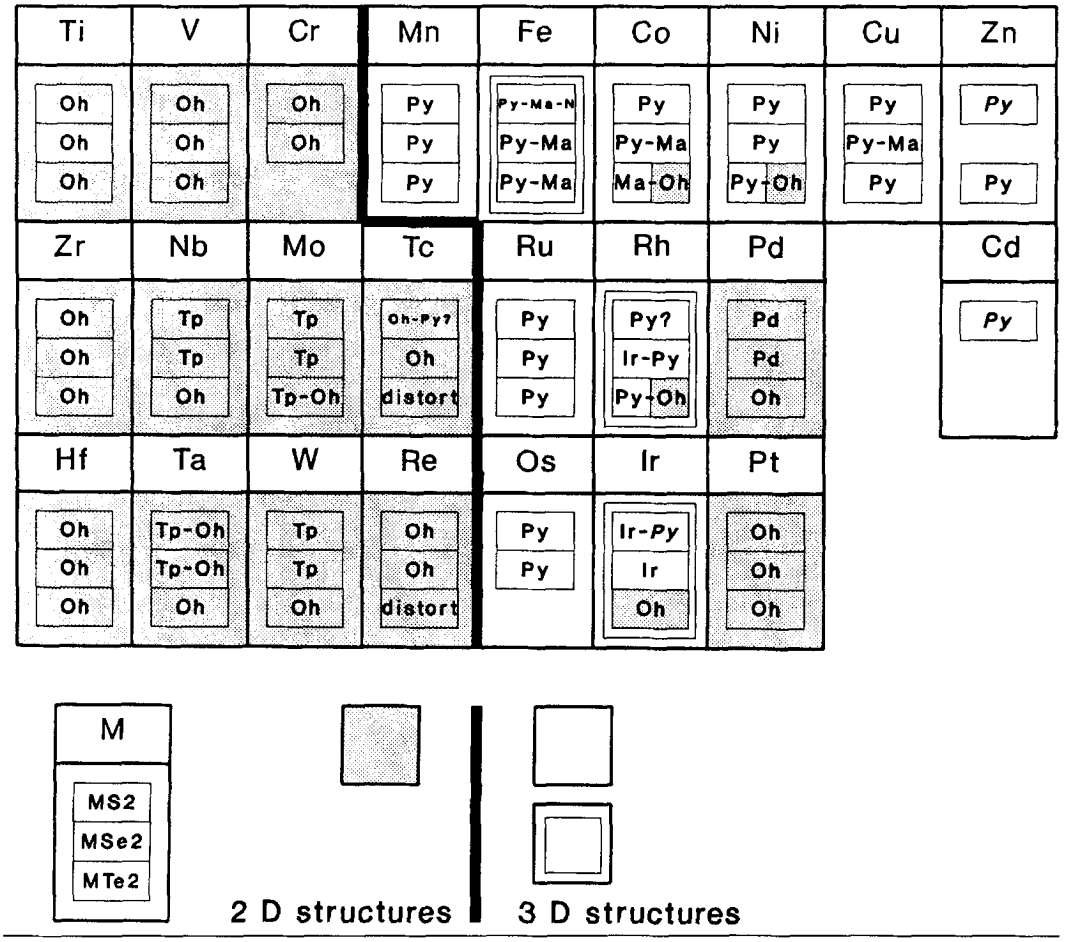

Note. For the 2D phases $(M^{4+}(X^{2-})_2)$ (shaded on figure), octahedral (Oh) and trigonal prismatic (Tp) coordination of the cation is indicated, while boxes with "distort" notation correspond to layer structure showing distorted environment. In the predominently 3D region, the $CoTe_2$, $NiTe_2$, $RhTe_2$, $IrTe_2$, PdX_2, and PtX_2 phases are 2D, PdS_2 and $PdSe_2$ exhibiting a specific arrangement (noted Pd) due to the special square coordination exerted by the palladium atoms. Most of the 3D materials present a pyrite (Py) or marcasite (Ma) structural type $(M^{2+}(X_2)^{2-})$ or $(M^{+}(X_2)^{-})$ (*5*) (bent letters indicate high pressure phases). Uncertainty about a structure type is noted by a question mark. A doubly framed area indicates the occurrence of special 3D structures $(M^{3+}X^{2-}(X_2^{2-})_{1/2})$ with half the anions present as X_2 pairs, either of the $IrSe_2$ type (noted Ir) or of the new FeS_2 type (noted N), this last one being obtained by soft chemistry (see text). The Ir and N structural types differ from the nature of the cationic site (respectively Oh and Td).

However, in the second family, there are several noticeable exceptions. The first one corresponds to PdX_2 phases (X = S, Se) (*2*), which exhibit a special layered structure. This is a variant of the pyrite structure resulting from elongating that structure in one direction so that Pd has four nearest and two more distant S (Se) neighbors instead of an octahedral group of six equidistant neighbors. Alternatively, the structure can be described as a layer structure, the layers consisting of Pd atoms forming four planar bonds to S_2 (Se_2) groups. The second exception is shown by the IrX_2 and $RhSe_2$ phases that present a particular case of tridimensional structure. The last exception is that of the $CoTe_2$, $NiTe_2$, $RhTe_2$, $PdTe_2$, $IrTe_2$, and PtX_2 phases with a reported CdI_2 structure, with, however, a very low c/a ratio of about 1.38.

It is worth pointing out that certain 2D materials can only be obtained through soft chemistry reactions, in particular VS_2 (*6, 7*), CrS_2 (*8*), and $CrSe_2$ (*9*), which are prepared by oxidation of AMX_2 ternary phases containing a mobile cation A^+ which is removed, with its electron, chemically or electrochemically at room or very moderate temperatures. A new kind of FeS_2 could also be obtained from Li_2FeS_2 through removal of the two lithium atoms (*10*). This new FeS_2 was characterized by Mössbauer, EXAFS, and Infra-Red methods (*11*) which, considering its rather amorphous nature, were the main possible investigative techniques.

These studies led to the charge balance $Fe^{3+}(Td)S^{2-}(S_2)^{2-}_{1/2}$, that is iron 3^+ cations in a tetrahedral environment, regular S^{2-} anions and $(S_2)^{2-}$ pairs, this last species occurring because of the oxidation of Li_2FeS_2. Clearly, this new iron disulfide has an electronic structure intermediate between those of the layered dichalcogenides, with a general formula $M^{4+}(S^{2-})_2$, and the pyrite-like phases $M^{2+}(S_2)^{2-}$. As in those compounds, the electronic feature of the new FeS_2 results from the competition between the anionic and the cationic oxidation states, that is between the relative stability of the cationic d orbitals and the anionic band levels. The position of iron in the Periodic Table, not very far from the frontier separating both structural groups, may explain this intermediate metastable situation. Since, due to the amorphous nature of the disintercalated material, the electronic structure of FeS_2 obtained by soft chemistry could only be put forward through spectroscopic studies, it was felt worthwhile to confirm the previous results by comparison with MX_2 compounds possibly related structurally to this compound.

In that respect and in agreement with the position of iridium in the Periodic Chart (near the transition border), the IrX_2 phases (X = S and Se) could be considered. In effect, the structural determination of $IrSe_2$ completed by X-ray diffraction analysis by L. B. Barricelli (*12*) showed the occurrence of Se–Se distances attributable to Se_2 pairs with the deduced $Ir^{3+}Se^{2-}(Se_2)^{-2}_{1/2}$ charge balance. IrS_2, with an apparently similar orthorhombic cell (only powder of this phase has so far been obtained), can also be thought to show the same kind of structure arrangement. IrS_2 might well thus present the very anionic features necessary for the projected comparative study, although, from a structural point of view, the filling of tetrahedral sites by Fe^{3+}, whereas Ir^{3+} is in octahedral ones, is a considerable difference. However, it seems that in both cases one is dealing with a similar case of competition between the cationic d levels and the anionic band. In order to compare the structures of the new FeS_2 and IrS_2 through Infra-Red spectroscopy, and to allow future electronic band calculations, the synthesis and structure characterization of IrS_2 (and also parent $IrSe_2$) were initiated. Rietveld structure determinations are given in this article.

Experimental

Both IrS_2 and $IrSe_2$ have been synthesized from the elements Ir, S, and Se used in stoichiometric proportions with iridium from Aldrich, 99.9% pure, selenium from Ventron, 99.99% pure and sulfur from Fluka, 99.999% pure. A dry box was used because of the high reactivity of iridium fine powder with oxygen. The evacuated silica tubes containing the elements were then heated at 900°C and 960°C (by steps of 100°C per day), respectively for $IrSe_2$ and IrS_2, the final temperature being maintained for 2 weeks before a 24-hr cooling to room temperature. Even with longer heating periods and/or higher temperature (up to 1100°C), no suitable single crystals could be grown. Attempts to obtain $IrSe_2$ single crystals through dissolution in a tellurium bath resulted in the complete substitution of Se by Te and in the preparation of Ir_3Te_8. The use of iodine as a transport agent failed to improve the size of the crystals to a point where they could have been used for single-crystal X-ray diffraction.

There exist several iridium chalcogenides, namely Ir_3S_8 (*13*) and Ir_3Se_8 (*14*), Ir_2S_3 (*15*) and $IrSe_3$ (*16*), and some nonstoichiometry has been reported for $IrSe_2$ (*12*). To ensure good homogeneity of the IrX_2 phases, grinding and refiring at the preparation temperatures were performed. This procedure resulted in no significant difference between samples, as shown from the refined cell parameters and spectral relative intensities. The disulfide derivative was annealed at 500°C with no change.

X-ray diffraction diagrams were obtained from an INEL curved detector and Cu$K\alpha$1 radiation (λ = 1.54059 Å) (silicium as standard). After ensuring a satisfactory purity of the phase and good powder diffraction lines, indexing, and parameter refining (*12, 17*), the samples were transferred to a Philips PW1820 diffractometer at the University of Reading where intensity data for the Rietveld structure determination were collected from Cu$K\alpha$ radiation using 10-sec counts at 0.02° intervals in the range 32–100° in 2θ for $IrSe_2$ and 29–92° for IrS_2. The data were subsequently refined by the Rietveld profile refinement technique using a program based on the Cambridge Crystallography Subroutine Library (*18*). The peak shape was modelled using a double Voigt function that accounted for Cu$K\alpha$1/$K\alpha$2.

Magnetic measurements were made with a Faraday balance (ASTEC-FRANCE) with a 1.7-T field. The samples were placed in a teflon holder. Electric conductivity were measured on bars of pressed powders using the Van der Pauw technique. The four contacts were made from silver glue.

Results and Discussions

It proved possible to index the $IrSe_2$ and IrS_2 powder pattern on the basis of the orthorhombic unit cell obtained from the $IrSe_2$ single crystal analysis by Barricelli (*12*) (Tables II and III). The total pattern could be accounted for. The least squares parameter refinement of $IrSe_2$ led to values for the cell dimensions of 20.955(2), 5.9381(6), 3.7429(4) Å, V = 465.7(1) Å^3. The average 2θ value deviation is 11/1000°, the reliability factor w being equal to 3.79×10^{-4}. The merit factors were set at $M(20) = 27$ and $F(20) = 28$. The same procedure was then used to index and refine the powder diffraction lines of IrS_2 with no lines rejected, indicating a fair purity of the phase. The refined cell dimensions were 19.791(1), 5.6242(5), 3.5673(3) Å with a volume of 397.1(1) Å^3. The w reliability factor was 2.65×10^{-4} with a mean 2θ difference of 10/1000°. Finally the figures of merit where equal to $M(20) = 28$ and $F(20) = 37$.

Details of the refinement of the cell dimensions are given in Table II for $IrSe_2$ and Table III for IrS_2. The cell dimensions are comparable to those obtained from the subsequent Rietveld refinement [$IrSe_2$,

TABLE II

$IrSe_2$ POWDER X-RAY DIFFRACTION DIAGRAM, WITH OBSERVED AND CALCULATED d_{hkl} VALUES. INTENSITIES ARE ESTIMATED

Compound: $IrSe_2$
Crystalline system: orthorhombic
Lattice parameters: a = 20.955(2) Å, b = 5.9381(6) Å, c = 3.7429(4) Å
Cell volume: V = 465.7(1) Å
Powder X-ray diffraction data:

$h\ k\ l$	d_{obs}	d_{cal}	I/I_{0obs}	$h\ k\ l$	d_{obs}	d_{cal}	I/I_{0obs}
2 0 0	10.44	10.47	8	0 0 2	1.8719	1.8715	28
1 1 0	5.69	5.71	21	4 3 0	1.8518	1.8516	15
2 1 0	5.1513	5.1661	2	9 2 0	1.8319	1.8322	15
3 1 0	4.5119	4.5242	36	10 0 1	1.8292	1.8285	5
4 1 0	3.9312	3.9285	21	1 1 2	1.7785	1.7785	2
2 0 1	3.5215	3.5248	0	0 3 1	1.7497	1.7498	37
5 1 0	3.4256	3.4241	38	1 3 1	1.7441	1.7437	3
4 0 1	3.0457	3.0455	84	3 1 2	1.7291	1.7294	5
0 2 0	2.9685	2.9690	14	3 3 1	1.6970	1.6973	3
1 2 0	2.9398	2.9397	13	4 1 2	1.6892	1.6895	4
2 2 0	2.8591	2.8566	2	5 1 2	1.6419	1.6422	15
4 1 1	2.7098	2.7099	36	5 3 1	1.6146	1.6147	3
4 2 0	2.5838	2.5831	20	0 2 2	1.5826	1.5832	7
6 0 1	2.5539	2.5535	11	1 2 2	1.5789	1.5787	6
5 1 1	2.5267	2.5264	18	13 1 0	1.5554	1.5557	16
5 2 0	2.4232	2.4227	14	4 2 2	1.5152	1.5155	8
1 2 1	2.3116	2.3119	2	5 2 2	1.4810	1.4811	7
3 2 1	2.2068	2.2069	2	14 1 0	1.4514	1.4514	4
7 1 1	2.1757	2.1753	16	1 4 1	1.3770	1.3770	2
9 1 0	2.1677	2.1677	2	1 3 2	1.3576	1.3570	0
8 0 1	2.1460	2.1461	1	8 2 2	1.3548	1.3549	10
4 2 1	2.1263	2.1260	28	10 3 1	1.3431	1.3431	2
10 0 0	2.0962	2.0955	1	7 4 0	1.3298	1.3300	1
5 2 1	2.0339	2.0338	23	13 2 1	1.3249	1.3249	5
8 1 1	2.0184	2.0183	14	4 3 2	1.3162	1.3163	12
8 2 0	1.9642	1.9643	7	9 2 2	1.3094	1.3092	17
9 1 1	1.8755	1.8758	100	5 3 2	1.2938	1.2935	1

Note. $w = 3.79 \times 10^{-4}$. Average 2θ angle deviation = 11/1000°. $M(20)$ = 27 and $F(20)$ = 28. The minimized w factor is: $w = 16/(n_p - n_v) \times ((\sin^2\theta_{cal} - \sin^2\theta_{obs} - D\theta_{ori} \sin^2\theta_{obs})/d\theta \sin 2\theta_{obs}))^2$, where n_p is the number of considered hkl planes and n_v the number of variables. θ_{cal} and θ_{obs} are the calculated and observed reflection angles. $d\theta$ is a prefixed angle shift (routinely equal to 0.03°) whereas $D\theta_{ori}$ is the origin shift (here taken equal to zero). Satisfactory w ranges generally from 5×10^{-4} downward.

The main figures of merit are $M(20)$ and $F(20)$ calculated respectively from the expressions: $M(n_r) = Q_r/2DQ_r\ n_c$ and $F(n_r) = 1/D2\theta \times n_r/n_c$ where n_r and n_c are the number of observed reflections and the number of possible reflecting planes. Q_r is $1/d^2_{hkl}$, DQ_r and $D2\theta$ are, respectively, the mean Q_r and 2θ shifts.

TABLE III

IrS_2 POWDER X-RAY DIFFRACTION DIAGRAM

Compound: IrS_2
Crystalline system: orthorhombic
Lattice parameters: a = 19.791(1) Å, b = 5.6242(5) Å, c = 3.5673(3) Å
Cell volume: V = 397.08(9) Å
Powder X-ray diffraction data:

$h\ k\ l$	d_{obs}	d_{cal}	I/I_{0obs}	$h\ k\ l$	d_{obs}	d_{cal}	I/I_{0obs}
2 0 0	9.85	9.90	9	5 2 1	1.9291	1.9286	40
1 1 0	5.39	5.41	23	8 1 1	1.9122	1.9119	16
4 0 0	4.9377	4.9479	2	8 2 0	1.8575	1.8575	12
2 1 0	4.8811	4.8897	2	6 2 1	1.8351	1.8351	3
3 1 0	4.2834	4.2800	40	0 0 2	1.7834	1.7837	35
4 1 0	3.7171	3.7149	28	9 1 1	1.7763	1.7762	80
2 0 1	3.3546	3.5759	0	4 3 0	1.7531	1.7531	31
6 0 0	3.2985	2.2986	2	9 2 0	1.7318	1.7323	27
5 1 0	3.2385	3.2370	62	5 3 0	1.6944	1.6943	8
0 1 1	3.0105	3.0125	9	0 3 1	1.6596	1.6595	46
1 1 0	2.9772	2.9781	44	1 3 1	1.6538	1.6537	9
4 0 1	2.8943	2.8936	100	3 1 2	1.6465	1.6464	14
0 2 0	2.8126	2.8121	19	6 3 0	1.6298	1.6299	2
1 2 0	2.7844	2.7842	21	10 2 0	1.6185	1.6185	2
3 1 1	2.7396	2.7403	1	4 1 2	1.6081	1.6079	12
2 2 0	2.7042	2.7050	2	5 1 2	1.5621	1.5622	27
4 1 1	2.5723	2.5731	11	5 3 1	1.5302	1.5305	2
8 0 0	2.4735	2.4739	8	0 2 2	1.5063	1.5062	13
4 2 0	2.4436	2.4448	5	1 2 2	1.5019	1.5019	14
6 0 1	2.4226	2.4219	11	12 0 1	1.4967	1.4970	11
5 1 1	2.3964	2.3972	15	13 1 0	1.4695	1.4695	31
5 2 0	2.2929	2.2925	9	8 0 2	1.4468	1.4468	9
8 1 0	2.2652	2.2645	0	4 2 2	1.4410	1.4409	4
6 1 1	2.2240	2.2244	1	5 2 2	1.4079	1.4077	8
1 2 1	2.1949	2.1948	4	1 4 0	1.4027	1.4025	7
3 2 1	2.0939	2.0942	10	8 3 1	1.3784	1.3782	18
7 1 1	2.0616	2.0616	10	14 1 0	1.3708	1.3710	4
9 1 0	2.0483	2.0481	2	10 3 0	1.3610	1.3611	3
8 0 1	2.0335	2.0329	0	10 0 2	1.3249	1.3250	12
4 2 1	2.0171	1.0167	42	12 2 1	1.3216	1.3215	7
10 0 0	1.9796	1.9791	6	14 0 1	1.3145	1.3142	6

Note. $w = 2.65 \times 10^{-4}$. Average 2θ angle deviation = 11/1000°. $M(20)$ = 28 and $F(20)$ = 37. Further comments as in Table II.

20.9451(8), 5.9351(3), 3.7406(2) Å; IrS_2, 19.7813(8), 5.6220(3), 3.5656(2) Å]. The zero points are −0.030(2)°, 0.000(2)° for $IrSe_2$ and IrS_2, respectively. The full width at half maximum and sample width were not refined directly (or independently). Instead the peak shapes were investigated using the Voigt function for both $\alpha 1$ and $\alpha 2$. The Gaussian contribution to this function σ was 0.042° and the Lorenzian contribution was $0.0136 \tan(\theta) + 0.0596 \sec(\theta)$. These quantities were refined for both compounds but came out to the same values.

For the Rietveld refinement, 269 reflec-

TABLE IV

POSITIONAL PARAMETERS ($\times 10^5$) OF $IrSe_2$ WITH ESTIMATED STANDARD DEVIATIONS IN PARENTHESES

Atom	x	y	z
Ir(1)	7,625(5)	43,001(22)	$\frac{1}{4}$
Ir(2)	30,501(6)	44,186(22)	$\frac{1}{4}$
Se(1)	36,083(13)	7,464(49)	$\frac{1}{4}$
Se(2)	37,797(14)	−45,389(45)	$\frac{3}{4}$
Se(3)	23,743(14)	31,995(49)	$\frac{3}{4}$
Se(4)	885(14)	27,250(47)	$\frac{3}{4}$

tions were used for $IrSe_2$ and 205 reflections for IrS_2. For both structures there were 53 basic variables made up of 3 cell dimensions, a scale factor, 9 background profile terms, 12 positional parameters, and 28 anisotropic thermal parameters terms.

Initial coordinates were based on the published structure for $IrSe_2$ in space group *Pnam* No. 62 (*12*). This structure determination was carried out on a single crystal but only *hk*0 and 0*kl* zones were measured from photographic data. The refinement (to R 0.17) was carried out in spacegroup *Pnam* with all atoms on mirror planes in the z direction but because of the limited amount of data, spacegroup $Pna2_1$ could not be ruled out.

In the present work, Rietveld refinement was successfully carried out for both structures [$IrSe_2$, 269 reflections, the weighted profile R-factor 0.062 compares well with an expected R factor of 0.032; IrS_2, 205 reflections; the weighted profile R factor 0.074 compares well with an expected R factor of 0.035]. The low χ^2 values of 3.81 and 7.03, respectively, indicate that both structures are well-modelled using space group *Pnam* (No. 62). There was no evidence from anisotropy in the thermal parameters that the structures were not consistent with mirror planes at $z = \frac{1}{4}$ and $\frac{3}{4}$. Final positional parameters for $IrSe_2$ and IrS_2 respectively are given in Tables IV and V, selected dimensions in Tables VI and VII, and anisotropic thermal parameters in Tables VIII and IX.

For IrS_2, many of the thermal parameters of the sulfur atoms converged to negative values. We suspect that this is because of our neglect of absorption. This is well apparent when considering the strong ESD of the sulfur coordinates (Table IX). Within 2 and 5 times the ESD values, the β' coefficients are all positive. Note that the considerable difference of weight between Ir and S must be considered to explain this anomaly. However these thermal parameters had negligible correlation with the positional parameters and so we consider the structure of IrS_2, as measured by bond lengths and angles, to be correct within the limits of the standard deviations.

The structures correspond to the previous determination (*12*) of the diselenide derivative with X^{2-} and $(X_2)^{2-}$ anionic groups; thus the structure can be described as a modification of the marcasite structure. As can be seen in Fig. 1a, the structure is built from IrX_6 octahedra sharing either two edges and two corners ($Ir_{(2)}X_6$) or three edges and one corner ($Ir_{(1)}X_6$). It can be observed that $(X_2)^{2-}$ pairs join four adjacent octahedra.

The marcasite structure would occur if anion–anion bonds appeared between $X_{(2)}$ and $X_{(4)}$ (see the broken lines on Fig. 1a), which is not the case as these chalco-

TABLE V

POSITIONAL PARAMETERS ($\times 10^5$) OF IrS_2 WITH ESTIMATED STANDARD DEVIATIONS IN PARENTHESES

Atom	x	y	z
Ir(1)	7,692(6)	42,399(25)	$\frac{1}{4}$
Ir(2)	30,376(7)	44,007(26)	$\frac{1}{4}$
S(1)	35,850(38)	6,124(145)	$\frac{1}{4}$
S(2)	37,532(33)	−45,312(125)	$\frac{3}{4}$
S(3)	23,691(41)	32,801(123)	$\frac{3}{4}$
S(4)	919(33)	27,304(117)	$\frac{3}{4}$

TABLE VI

BOND DISTANCES (IN Å) AND ANGLES (IN DEGREES) AROUND THE METAL FROM $IrSe_2$ STRUCTURE REFINEMENT WITH e.s.d's IN PARENTHESES

(a) Principal bond distances (in Å).		
Ir(1)–Se(1)	2.445(2) (×2)	
Ir(1)–Se(2)	2.473(3)	
Ir(1)–Se(4)	2.524(3) (×2)	
Ir(1)–Se(4)	2.510(3)	
Ir(2)–Se(1)	2.475(3)	
Ir(2)–Se(3)	2.415(3)	
Ir(2)–Se(2)	2.495(3) (×2)	
Ir(2)–Se(3)	2.456(2) (×2)	
Average Ir–Se distance: 2.476(3)		
Pair	Se(3)–Se(1)	2.555(4)
Smallest Se . . . Se nonbonded distance		
	Se(3)–Se(2)	3.237(2)
Closest Ir . . . Ir distance		
	Ir(1)–Ir(1)	3.743
(b) Angles (°) around the metal atoms.		
Cis angles		
Se(1)–Ir(1)–Se(2)		96.6(1) (×2)
Se(1)–Ir(1)–Se(4)		82.2(1) (×2)
Se(1)–Ir(1)–Se(1)		99.9(1) (×2)
Se(2)–Ir(1)–Se(4)		82.9(1) (×2)
Se(4)–Ir(1)–Se(4)		82.1(1) (×2)
Se(1)–Ir(1)–Se(4)		97.8(1)
Se(4)–Ir(1)–Se(4)		95.7(1)
Trans angles		
Se(4)–Ir(1)–Se(1)		177.9(1) (×2)
Se(2)–Ir(1)–Se(4)		157.6(1)
Cis angles		
Se(1)–Ir(2)–Se(2)		85.9(1) (×2)
Se(1)–Ir(2)–Se(3)		90.7(1) (×2)
Se(3)–Ir(2)–Se(2)		89.7(1) (×2)
Se(3)–Ir(2)–Se(3)		93.5(1) (×2)
Se(2)–Ir(2)–Se(3)		81.7(1) (×2)
Se(2)–Ir(2)–Se(2)		97.2(1)
Se(3)–Ir(2)–Se(3)		99.3(1)
Trans angles		
Se(2)–Ir(2)–Se(3)		176.5(1) (×2)
Se(1)–Ir(2)–Se(3)		173.4(1)

TABLE VII

BOND DISTANCES (IN Å) AND ANGLES (IN DEGREES) AROUND THE METAL FROM IrS_2 STRUCTURE REFINEMENT WITH e.s.d's IN PARENTHESES

(a) Principal bond distances (in Å).		
Ir(1)–S(1)	2.326(5) (×2)	
Ir(1)–S(2)	2.322(7)	
Ir(1)–S(4)	2.387(5) (×2)	
Ir(1)–S(4)	2.410(7)	
Ir(2)–S(1)	2.390(8)	
Ir(2)–S(3)	2.326(7)	
Ir(2)–S(2)	2.355(5) (×2)	
Ir(2)–S(3)	2.309(5) (×2)	
Average Ir–S distance: 2.350(6)		
Pair	S(3)–S(1)	2.299(11)
Smallest S . . . S nonbonded distance		
	S(3)–S(2)	3.003(10)
Closest Ir . . . Ir distance		
	Ir(1)–Ir(1)	3.567
(b) Angles (°) around the metal atoms.		
Cis angles		
Se(1)–Ir(1)–S(2)		94.6(2) (×2)
S(1)–Ir(1)–S(4)		81.6(2) (×2)
S(1)–Ir(1)–S(1)		100.1(2) (×2)
S(2)–Ir(1)–S(4)		84.5(1) (×2)
S(4)–Ir(1)–S(4)		81.6(1) (×2)
S(1)–Ir(1)–S(4)		98.9(2)
S(4)–Ir(1)–S(4)		96.7(1)
Trans angles		
S(4)–Ir(1)–S(1)		178.1(2) (×2)
S(2)–Ir(1)–S(4)		159.0(2)
Cis angles		
S(1)–Ir(2)–S(2)		87.4(2) (×2)
S(1)–Ir(2)–S(3)		90.9(2) (×2)
S(3)–Ir(2)–S(2)		88.2(2) (×2)
S(3)–Ir(2)–S(3)		93.3(2) (×2)
S(2)–Ir(2)–S(3)		80.2(2) (×2)
S(2)–Ir(2)–S(2)		98.5(2)
S(3)–Ir(2)–S(3)		101.2(2)
Trans angles		
S(2)–Ir(2)–S(3)		177.9(2) (×2)
S(1)–Ir(2)–S(3)		173.3(2)

gen–chalcogen distances are much longer than a bond length (e.g., $Se_{(2)} \ldots Se_{(4)}$ = 3.330(4) Å in $IrSe_2$ and $S_{(2)} \ldots S_{(4)}$ = 3.203(9) Å in IrS_2).

Looking at the values of the distances and angles given in Tables VI and VII, the following conclusions can be drawn.

—The two $[IrS_6]$ and $[IrSe_6]$ octahedra are strongly distorted with *cis* angles ranging from 99.9(1)° to 81.7(1)° for $IrSe_2$ and 101.1(2)° to 80.2(2)° for IrS_2. These distortions go along with significant variations in Ir–*X* bond lengths which range from 2.415(3) Å to 2.524(3) Å and from 2.309(5)

TABLE VIII

ANISOTROPIC THERMAL PARAMETERS ($\times 10^4$) IN THE FORM $\exp -(2\pi^2(B_{11} \cdot h^2 \cdot a^{*2} + B_{22} \cdot k^2 \cdot b^{*2} + \ldots + 2B_{12} \cdot h \cdot k \cdot a^* \cdot b^* + \ldots))$ FOR $IrSe_2$ WITH ESTIMATED STANDARD DEVIATIONS IN PARENTHESES

Atom	B_{11}	B_{22}	B_{33}	B_{12}
Ir(1)	1.64(6)	1.64(6)	1.66(6)	0.06(6)
Ir(2)	1.44(5)	1.73(5)	1.25(5)	0.04(5)
Se(1)	1.09(12)	1.46(12)	0.61(12)	0.41(12)
Se(2)	1.46(10)	1.01(10)	0.92(10)	0.17(10)
Se(3)	1.39(11)	0.89(11)	0.97(11)	−0.50(11)
Se(4)	1.37(12)	1.06(12)	1.16(12)	0.00(12)

Å to 2.410(7) Å. It can be noted that one of the *trans* angles for $Ir_{(1)}$ [$X_{(2)}$–Ir–$X_{(4)}$ X = Se 157.6(1)°, X = S 159.0(2)°] is considerably more distorted away from 180° than the other trans angles, which all fall within the range 173–180°, in the two metal octahedra.

—The average Ir–Se and Ir–S bond distances are equal to 2.476 and 2.350 Å. Using an effective ionic radius (EIR) of 1.98 and 1.84 Å (*19*) for Se^{2-} and S^{2-}, respectively,[1] the ionic radius of Ir^{3+} works out to be 0.50 and 0.51 Å in the two structures. The radii are significantly smaller than the accepted value of r = 0.68 Å (*19, 20*) calculated or observed for Ir^{3+}, but are in remarkable agreement with each other, underscoring the overall consistency of the structure determinations. Such a small calculated cation size is also observed in related rhodium chalcogenides (*13*). In effect, Rh_3Se_8, with a defect pyrite structure, gives an average Rh–Se distance of 2.50 Å, yielding a cation size of 0.52 Å, much smaller than literature values ($r^{3+}_{(Rh)}$) = 0.67 Å from (*19, 20*)).

—The chalcogen–chalcogen distances of the X_2 pairs, i.e., $Se_{(1)}$–$Se_{(3)}$ = 2.555(4) Å and $S_{(1)}$–$S_{(3)}$ = 2.299(11) Å, exceed the usual values. For regular pairs, distances for Se–Se of ca. 2.35 Å (*21–23*) and for S–S of ca. 2.05 Å (*24–27*), have been observed in semiconducting phases, i.e., about 10% smaller. Longer bond distances as observed in $IrSe_2$ and IrS_2 have also been reported in $RhSe_2$ (Se–Se = 2.50 Å) (*28*), in $TaSe_3$ (Se–Se = 2.576 Å) (*29*), in $NbSe_3$ (Se–Se = 2.49 and 2.91 Å) (*30*) and in FeS_2 marcasite (S–S = 2.21 Å) (*31*). Variations in the chalcogen–chalcogen bond length can be related to the filling of antibonding levels of the X_2 pairs (*32*). For the IrX_2 phases, to be described in a first approach as $Ir^{3+}X^{2-}(X_2)^{2-}_{1/2}$, this could correspond to some electron transfer from iridium to the X_2 pair, pushing the phase toward a more CdI_2 charge balance type of structure. However, within that scheme, one would expect the occurrence of some paramagnetism at the iridium and pair sites.

In order to study that possibility, magnetic susceptibility measurements were performed between 80 and 400 K. They showed a fairly constant diamagnetism of $x = -9 \times 10^{-5}$ emu/mol for IrS_2 and of $x = -1.6 \times 10^{-4}$ emu/mol for $IrSe_2$, in reasonable agreement with the known diamagnetism of the ionic species. This result is in accord with a previous report (*12*) and is consistent with the chalcogen pairing and increased covalent interactions which imply a low spin d^6 configuration for Ir^{3+}. This is a situation

TABLE IX

ANISOTROPIC THERMAL PARAMETERS ($\times 10^4$) IN THE FORM $\exp -(2\pi^2(B_{11} \cdot h^2 \cdot a^{*2} + B_{22} \cdot k^2 \cdot b^{*2} + \ldots + 2B_{12} \cdot h \cdot k \cdot a^* \cdot b^* + \ldots))$ FOR IrS_2 WITH ESTIMATED STANDARD DEVIATIONS IN PARENTHESES

Atom	B_{11}	B_{22}	B_{33}	B_{12}
Ir(1)	0.41(9)	−0.10(9)	0.72(10)	−0.18(7)
Ir(2)	0.10(8)	0.46(8)	0.40(8)	0.06(7)
S(1)	0.75(47)	−0.64(41)	−1.58(41)	−0.21(40)
S(2)	−1.13(35)	−1.03(37)	−1.19(37)	0.51(33)
S(3)	−0.70(44)	−0.02(46)	−0.92(44)	−1.44(30)
S(4)	−1.76(35)	−1.79(36)	0.47(52)	−0.53(31)

[1] These radii are used also for the chalcogen bonded in pairs since there is no apparent difference in Ir–X lengths in the structure. This was also done in other pairs containing phases with satisfactory radius calculations (*24–27*).

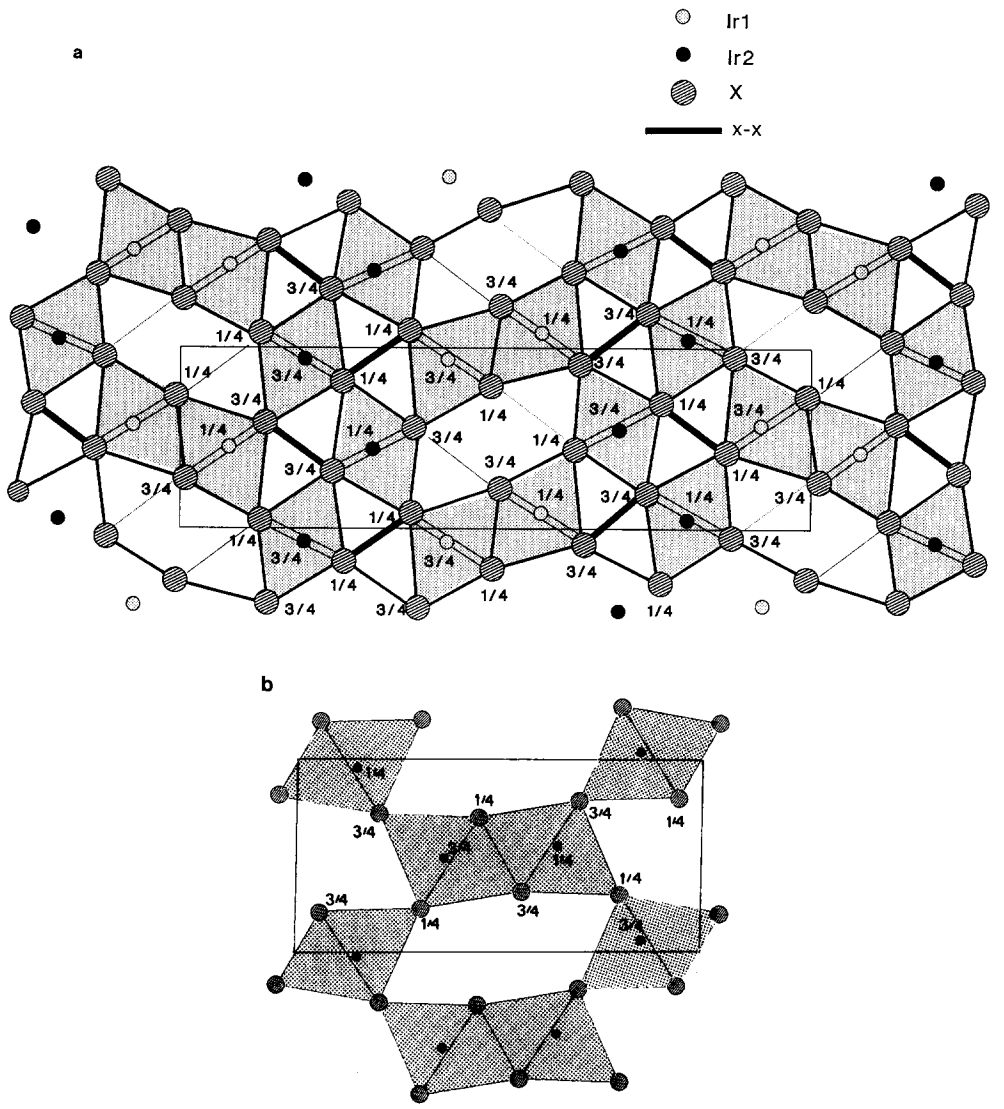

FIG. 1. (a) Structure of IrX_2 showing IrX_6 octahedra sharing either two edges and two corners ($Ir_{(2)}X_6$) or three edges and one corner ($Ir_{(1)}X_6$). (b) Projection of the unit cell of the Ramsdellite type structure (as exhibited by MnO_2 for instance), showing the occurrence of similar blocks in IrX_2.

similar to Fe^{2+} in pyrite and the low spin suggests here also an eg–π^* interaction raising the eg band level, such a rise being responsible for the electronic configuration. The structure and the charge balance of the IrX_2 phases seem thus confirmed.

However, the reason for the long Se–Se and S–S distances remains to be considered.

One possible explanation is that the elongation is caused by strains in the structure. As reported earlier, there are considerable distortions of the IrX_6 octahedral groups and these would be considerably greater with shorter (and more usual) chalcogen–chalcogen distances. Extra evidence of the tension in the phase is given by the rather short

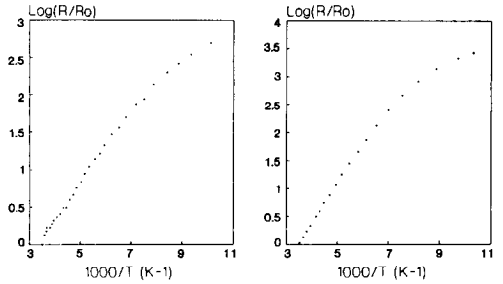

FIG. 2. Electrical behavior of $IrSe_2$ and IrS_2 versus temperature. Determination of the activation energy from the relation $\sigma^{-1} = \sigma_0^{-1} \times \exp(E/2kT)$.

distances of neighbor nonbonded chalcogens (e.g. $X_{(3)} \ldots X_{(2)}$ X = Se 3.237(4), X = S 3.003(9) Å), whereas the sum of the established covalent chalcogen radii would lead to about 3.96 and 3.68 Å. Note also that short sulfur–sulfur contact distances of d_{S-S} = 2.995 and 2.972 Å were found in PV_2S_{10}, for instance, and were ascribed to steric effects (*33*). Such a steric effect could also be at play in IrS_2 and $IrSe_2$ but this would not explain the very small cation radius observed for Ir^{3+}.

To complete our study and confirm the above results, conduction measurements (Fig. 2) were performed on pressed samples of the two iridium phases. The high temperature part of the curve of $\mathrm{Ln}(R/R_0)$ versus $1/T$ shows a linear variation allowing the calculation [from $\sigma^{-1} = \sigma_0^{-1} * \exp(E/2kT)$] of activation energies of respectively E = 0.13 and 0.09 eV for IrS_2 and $IrSe_2$. Although the phases show a conductivity variation of the semiconducting type, the room temperature resistivity (σ^{-1}_{IrS2} = 45 Ω cm and σ^{-1}_{IrSe2} = 11 Ω cm) is quite low, as the activation energy also is. These results support the overall charge distribution of the phase as inferred above, but raise the question of such a high charge carrier mobility. It is possible that the origin of this phenomenon comes from polaronic conduction in relation with either some nonstoichiometry on the anionic sites or anionic S^{-2} and $(S_2)^{-2}$ band overlap. To try to answer that question, it may be of interest to go back to the abnormally small radius of L.S. Ir^{3+} as calculated from the effective radius of Se^{2-} and S^{2-}.

Since a long X–X bond distance is observed, this suggests an electron filling of an antibonding level (of σ^* character for example) of the X–X pairs, possibly inducing a high conductivity for the compound. To test that hypothesis, let us consider for instance CuS_2 and FeS_2 pyrite for which the oxidation state of the S_2 groups (S_2^{-1} and S_2^{-2}) is well established (*5*). The two distances of 2.03 and 2.13 Å for CuS_2 and FeS_2 sulfur pairs can be placed on a diagram of d_{S-S} versus the chalcogen oxidation state. A straight line can be obtained for the 2.30 Å pair bond length of IrS_2 if one considers the occurrence of $(S_2)^{-3}$ pairs (Fig. 3).

This would lead to the formation of $S^{-3/2}$ monoatomic groups in agreement with the charge balance $Ir^{3+}S^{-1.5}(S_2^{-3})_{1/2}$, giving the same negative charge on all the anions. These results present several advantages. They explain why there is no dispersion of the Ir–S distances in the (IrS_6) octahedra allowing one to distinguish between the two anionic species. A smaller effective radius for sulfur is to be considered in particular for the monoanions allowing the calculation of a more correct Ir^{3+} cationic radius. Holes may be created in the structure bands explaining the high conductivity and weak activation energy. These results seem to hold for the selenide phase as well.

Conclusion

After Rietveld structure determinations, several unexpected and, in some respect, abnormal characteristics in the structure of IrS_2 and $IrSe_2$ were pointed out along with physical properties. Putting aside a possible strain within the structure to be related to steric effects, an internal redox process can

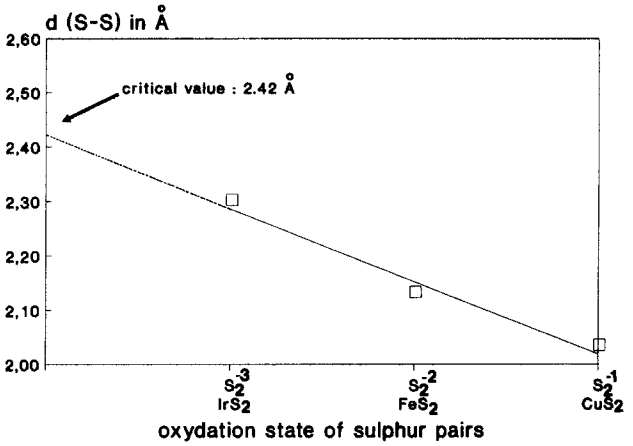

FIG. 3. Variation of the S–S bond distance of anionic pairs in dichalcogenides of Cu, Fe, and Ir versus sulfur oxidation state. A straight line is obtained assuming an oxidation state of $-$III for the S_2 pair of IrS_2. From the curve, a critical distance of approximately 2.42 Å can be extrapolated. It could correspond to the breaking of the pair bond.

be suggested between the different anions of the structure, in relation to the X–X bond distances. The proposed electronic transfer could result in holes, possibly responsible of the electronic properties, occurring within the anionic bands. A band structure calculation on IrS_2 and $IrSe_2$ and Hall and thermoelectric effects measurements should shed some light on these assumptions.

Acknowledgments

We thank Dr. A. Porker, Postgraduate Research Institute in Sedimentology, University of Reading for measuring powder data.

References

1. M. S. WHITTINGHAM, *Prog.Solid State Chem.* **12,** 41 (1978).
2. "Crystallography and Crystal Chemistry of Material with Layered Structures," Vol. 2, Reidel, Dordrecht, Holland (1976).
3. J. BENARD AND Y. JEANNIN, *Adv. Chem. Ser. (Amer. Chem. Soc.)* **39,** 191 (1962).
4. A. GLEIZES AND Y. JEANNIN, *Solid State Chem.* **1,** 180 (1970).
5. J. C. W. FOLMER, F. JELLINEK, AND G. H. M. CALIS, *J. Solid State Chem.* **72,** 137 (1988).
6. D. W. MURPHY, J. N. CARIDES, F. J. DI SALVO, C. CROS, AND J. V. WASZCZAK, *Mater. Res. Bull.* **12,** 825 (1977).
7. D. W. MURPHY AND J. N. CARIDES, *J. Elec. Soc.* **126,** 749 (1979).
8. V. MANEV, R. V. MOSHTEV, A. NASSALEVSKA, AND G. PISTOIA, *Solid State Ionics* **13,** 181 (1984).
9. C. F. VAN BRUGGEN, R. J. HAANGE, G. A. WIEGERS, AND D. K. G. DE BOER, *Physica* **99B,** 166 (1980).
10. R. BREC, G. OUVRARD, AND E. PROUZET, *J. Power Sources* **26,** 319 (1989).
11. L. BLANDEAU, G. OUVRARD, Y. CALAGE, R. BREC, AND J. ROUXEL, *J. Phys. C: Solid State Phys.* **20,** 4271 (1987).
12. L. B. BARRICELLI, *Acta Crystallogr.* **11,** 75 (1958).
13. D. HOHNKE AND E. PARTHE, *Z. Kristallogr.* **127,** 164 (1968).
14. A. KJEKSHUS, J. RAKKE, AND A. ANDRESEN, *Acta Chem. Scand.* **A32,** 209 (1978).
15. E. PARTHÉ, D. HOHNKE, AND F. HULLIGER, *Acta Crystallogr.* **23,** 832 (1967).
16. E. PARTHÉ AND D. HOHNKE in "The Chemistry of Extended Defects in Non-Metallic Solids," (L. Eyring and M. O'Keeffe, Eds.), p. 220, North Holland, Amsterdam (1970).
17. F. HULLIGER, *Nature (London)* **204** (1964).
18. W. I. F. DAVID, D. E. AKPORIAYE, R. MIBBERSON, AND C. C. WILSON, Rutherford Appleton Laboratory Report RAL-88-103 (1988).
19. R. D. SHANNON, *Acta Crystallogr.* **32,** 751 (1976).
20. R. D. SHANNON, "Structure and Bondings in Crys-

tals," Vol. II, pp. 53–69, Academic Press, San Diego (1981).
21. M. EVAIN, M. QUEIGNEC, R. BREC, AND C. SOURISSEAU, *J. Solid State Chem.* **75,** 413 (1988).
22. A. MEERSCHAUT, L. GUÉMAS, R. BERGER, AND J. ROUXEL, *Acta Crystallogr.* B35, 1747 (1979).
23. A. MEERSCHAUT, P. PALVADEAU, AND J. ROUXEL, *J. Solid State Chem.* **20,** 21 (1977).
24. R. BREC, G. OUVRARD, M. EVAIN, P. GRENOUILLEAU, AND J. ROUXEL, *J. Solid State Chem.* **47,** 174 (1983).
25. R. BREC, M. EVAIN, P. GRENOUILLEAU, AND J. ROUXEL, *Rev. Chim. Miner.* **20,** 283 (1983).
26. R. BREC, P. GRENOUILLEAU, M. EVAIN, AND J. ROUXEL, *Rev. Chim. Miner.* **20,** 295 (1983).
27. M. EVAIN, M. QUEIGNEC, R. BREC, AND J. ROUXEL, *J. Solid State Chem.* **56,** 148 (1985).
28. S. GELLER AND B. B. CETLIN, *Acta Crystallogr.* **8,** 272 (1955).
29. E. BJERKELUND, J. H. FERMOR, AND A. KJEKSHUS, *Acta Chem. Scand.* **20,** 1836 (1966).
30. A. MEERSCHAUT AND J. ROUXEL, *J. Less-Common Met.* **39,** 197 (1975).
31. G. BROSTIGEN, A. KJEKSHUS, AND C. H. R. ROMMING, *Acta Chem. Scand.* **27,** 2791 (1973).
32. H. VAN DER HEIDE, R. HEMMEL, C. F. VAN BRUGGEN, AND C. HAAS, *J. Solid State Chem.* **33,** 17 (1980).
33. M. EVAIN, Thesis, University of Nantes (1986), France.